EVLA Memo #154
Characterization of the EVLA 1-2 GHz Intermediate Frequency Passband (Updated)*

Keith Morris and Emmanuel Momjian (NRAO)

January 23, 2012

Abstract

The EVLA 1-2 GHz Intermediate Frequency (IF), as presented to the 8-bit sampler, shows characteristic bandpass shapes that are independent of receiver band, upconverter path, or sideband. The implication is that the T304 baseband converter imprints its own characteristic response on the IF signal. This memo seeks to identify the causes of this characteristic shape, and to identify (where possible) or dismiss (where necessary) potential solutions.

1 Introduction

Early wide-band observations with the EVLA L-band (1-2 GHz) receiver using the 8-bit signal path showed a noticeable loss of sensitivity at the lower ∼100 MHz. This was initially attributed to the L-band receiver response (e.g., EVLA Memo #152; Momjian & Perley 2011). However, observations using other EVLA receivers show the same behavior, and lab tests confirm that this effect is independent of any receiver band. Further studies have shown that much of this behavior originates in the downconverter (T304).

The input band of the T304 nominally spans 8-12 GHz, of which a 1 GHz-wide Intermediate Frequency (IF) window will appear at its output and will be presented to the 1 GHz-wide digitizer. For the purpose of this analysis, we partition the 8-12 GHz input band into four 1 GHz IF windows, each accessible by a particular tuning of the 2nd LO synthesizer (L302) as seen in Figure 1. For convenience, these windows will be referred to by the numbering scheme listed in Table 1.

Window	Intermediate Frequency (IF) (GHz)	2nd LO (L302) frequency (GHz)
1	8 - 9	11.022
2	9 - 10	12.047
3	10 - 11	13.072
4	11 - 12	14.097

Table 1: The four 1 GHz windows and their respective 2nd LO frequencies. The LO frequencies are chosen in order to provide four equally spaced 1 GHz windows that cover the 4 GHz input to the downconverter (T304).

*The original version of this memo assumed a WIDAR subband 0 filter response that has not yet been implemented in the system. Information about this filter's current implementation has surfaced since the original publication of this memo. This revision, dated January 23, 2012, accurately reflects the current state of the system as described in §2, §4.1, and §5

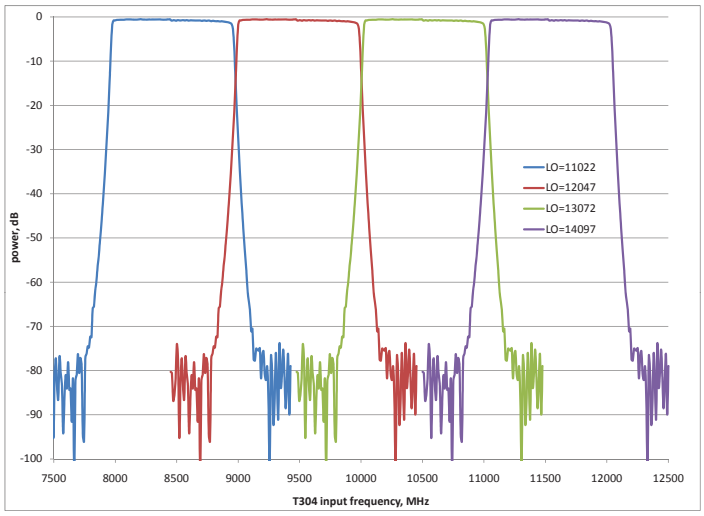

Figure 1: The four 1 GHz windows for an ideal T304 frequency response mapped to the T304 input frequency.

Test observations have shown that the loss of sensitivity at the band edge was exaggerated at one of these tunings: window 4. Figure 2 highlights this loss of sensitivity, which affects about 60% of the usable 1 GHz bandwidth. The loss of sensitivity is only ∼4% for the most part of the affected band, but it is much more significant (> 10%) for the outer 128 MHz (i.e., subband 0 of the 4th 1 GHz window, see §2). While this is a potential problem for all the frequency bands of the EVLA, it is unavoidable for both L-band (1-2 GHz) and X-band (8-12 GHz). For L-band, the 1st LO (L301) tuning forces the use of the 4th 1 GHz window. For X-band, which doesn't use the L301, the highest 1 GHz coincides with this window.

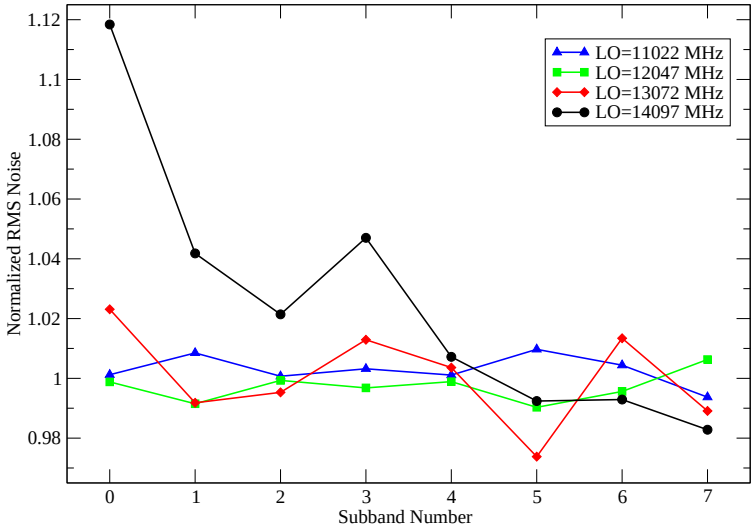

Figure 2: The normalized RMS noise values of each WIDAR subband in each of the four windows using a set of EVLA antennas equipped with the Ku-band receivers. The data points are of the average RMS noise values of the central 10 channels (20 MHz) in each 128 MHz-wide subband normalized by the average of the values obtained from both the 1st and 2nd 1 GHz windows for each subband. The LO frequencies refer to the L302 (see Table 1).

Our tests reveal that the loss of sensitivity noted above is associated with a characteristic bandpass shape in the sampled IF that has three distinct features:

1. A general slope across the passband, which we refer to as *slope*. The slope is most noticeable in the 4th window.

2. A pronounced roll-off on the 2 GHz edge of the passband (subband 0), which we refer to as *shoulder*. The shoulder is also most noticeable in the 4th window.

3. An asymmetry in the outer ∼30 MHz of each edge of the passband, which we refer to as *asymmetry*, and does not depend on choice of window.

Each of these effects has a distinct cause in the system. For illustration, Figure 3 shows the four 1 GHz windows, from a typical on-the-sky observation, overlaid. Each window is split into eight 128 MHz-wide subbands by the WIDAR correlator, each with 64 spectral channels. This figure schematically indicates the location of each of the three effects listed above. All three effects become more evident in the 4th window (14097 MHz; black trace).

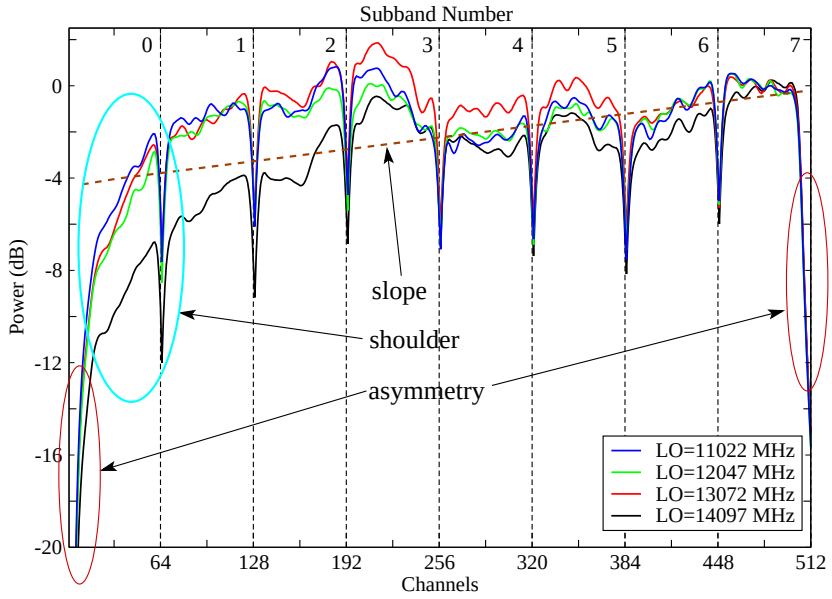

Figure 3: The bandpass shape of the four 1 GHz windows for a single polarization (RCP) of antenna EA22. The amplitude values have been normalized using the central 10 channels (20 MHz) of subband 7 in each 1 GHz window. The plots highlight the three issues that are affecting the 1-2 GHz IF passband: the general slope across the passband (*slope*), the pronounced roll-off on the 2 GHz edge of the band (*shoulder*), and the asymmetry in the steepest edges of the passband (*asymmetry*). Note that these effects are independent of polarization.

2 Background

Figure 4 is a simplified block diagram of the T304 that shows the location of the frequency mixers and filters that convert a 1 GHz IF window from the 8-12 GHz T304 input signal to the 1-2 GHz digitizer input signal. In February 2008, the T304 downconverter was found to have a cascade of filters that was allowing unwanted signal to leak through the 2nd conversion mixer and into the

sampled baseband. The unwanted signal was $10-15$ dB below the astronomical signal, in violation of the EVLA Project Book specification for image rejection of 30 dB. Figure 5 shows the response of these filters overlaid with the response of the anti-aliasing filter to enable visual comparison. The highpass filter, shown in orange, allows signal in-band to the samplers to leak directly through the mixer. Swept measurements on a Scalar Network Analyzer (SNA) allowed us to unwrap the leakage signal from the signal of interest. This is shown in Figure 6.

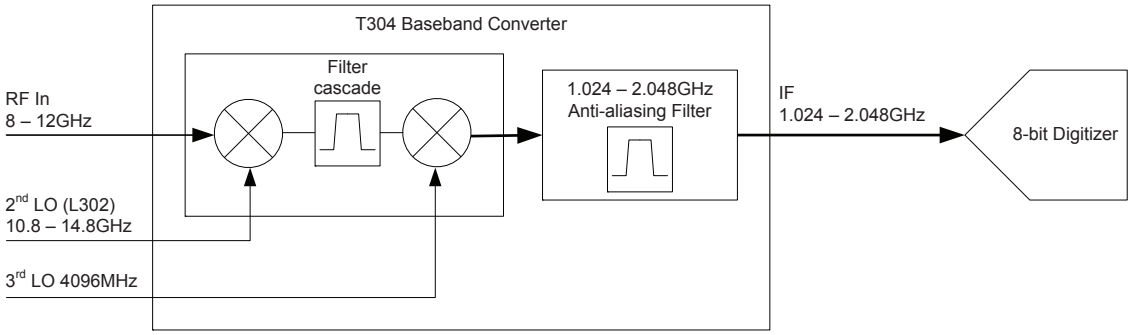

Figure 4: Simplified block diagram showing the T304 and the digitizer. The filter cascade located before the 2nd mixer selects the band of frequencies which, after conversion, will match the anti-aliasing filter passband.

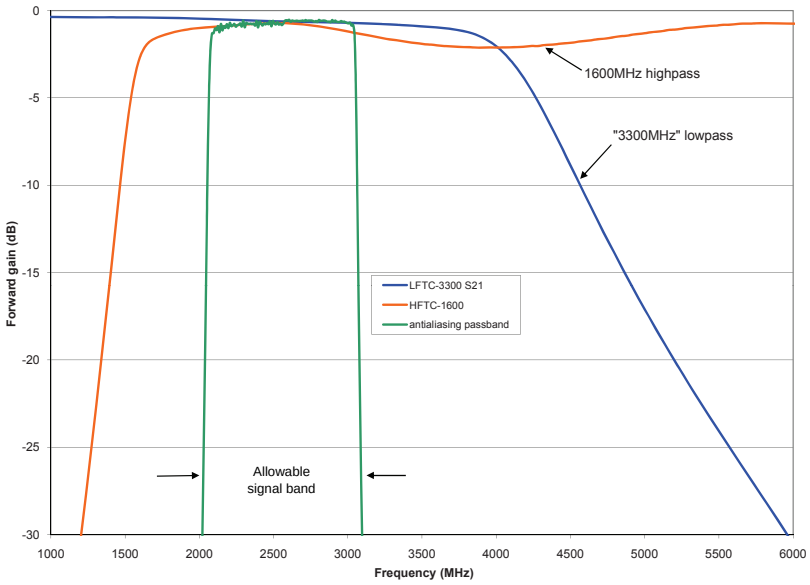

Figure 5: T304 filter cascade before modification. The 1600 MHz highpass filter (orange trace) and the 3300 MHz lowpass filter (blue trace) together form a bandpass filter that is intended to limit the bandwidth of the signal entering the mixer. The green trace represents the anti-aliasing filter which has been numerically upconverted with the 4096 MHz fixed LO to enable visual comparison.

The manufacturer of the 1600 MHz highpass filter produces pin-compatible alternatives with four different cutoff frequencies; only one of these, the 1900 MHz, eliminated the unwanted signal while passing the signal of interest. Upon replacing the highpass filter, it was discovered that the 2 GHz edge (subband 0) of the digitized signal suffered from an unexpected and asymmetric roll-off on the order of 1 to 2 dB over the outer 30 MHz. This effect was not seen initially because the EVLA transition LO system, which used the EVLA antennas with the old VLA correlator, placed the observable 50 MHz-wide sky signal in subband 6.

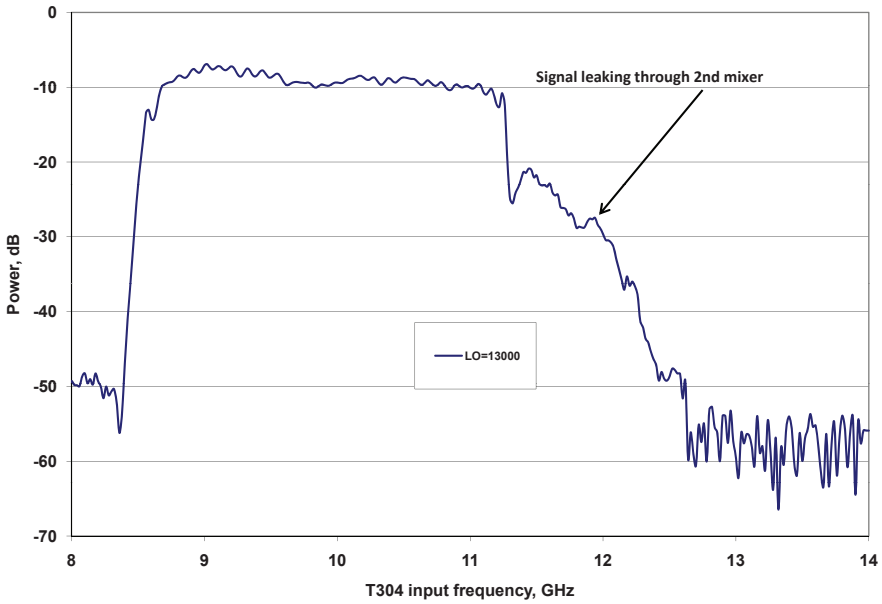

Figure 6: Mixer signal leakage in the T304. The signal between ∼11.3 and 12.1 GHz corresponds to the region bounded by the orange and green traces (∼1200 to 2000 MHz) shown in Figure 5.

The 1900 MHz highpass filter not only blocks the unwanted signal but also a small amount of the desired signal. This is evident in Figure 7, where the orange trace intersects the green trace at ∼2000 MHz. It was decided at the time that this small roll-off was an acceptable price to pay for the elimination of the corrupted signal.

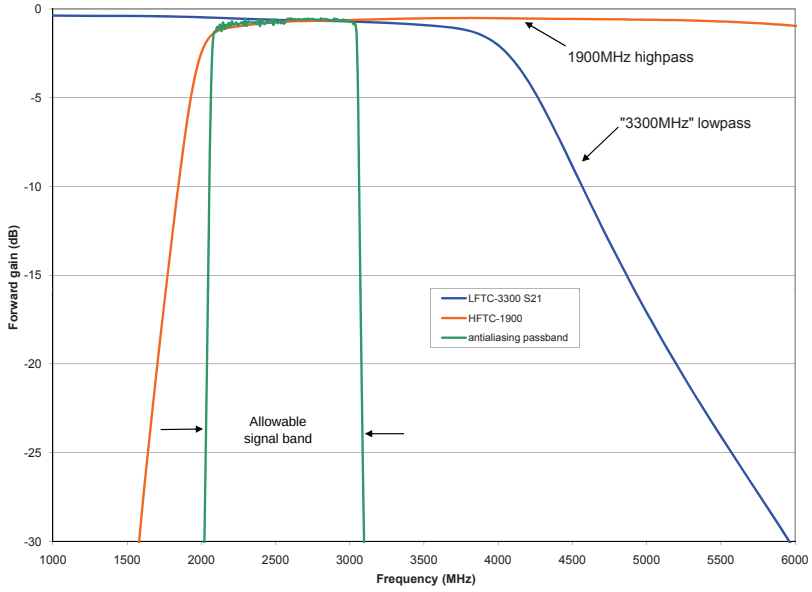

Figure 7: T304 filter cascade after modification. Mixer signal leakage has been suppressed, but some unwanted band-edge roll-off was introduced.

The difference between the old and new highpass filters was illustrated recently during on-the-sky testing of the array at Q-band. Figure 8 shows the spectra seen by the deformatter of antenna 21 during these observations. The T304 modules in three of the four basebands – A, C, and D – had all received the updated highpass filter. The module for baseband B is still in place from its original installation in 2007, and had never returned to the lab for retrofitting with the new

filter. This module, though its bandpass looks preferable to the other three, fails to meet the image rejection specification and must be modified, sacrificing its sharper bandpass corner to meet the EVLA project requirements.

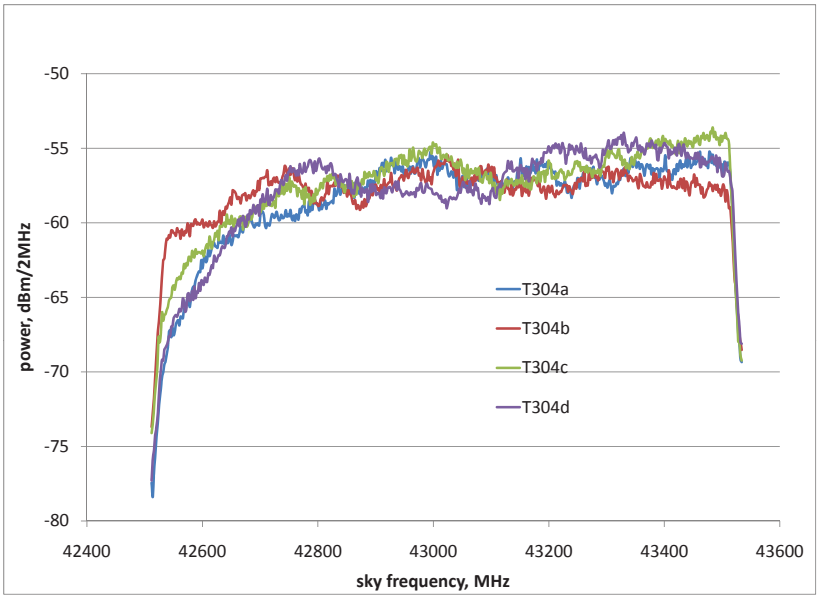

Figure 8: Spectra taken with the bandpass plotting tool of the four basebands of antenna 21 during Q-band observations. Basebands A, C, and D use modern T304s, and all show the shoulder effect, while baseband B (red trace) has a much sharper filter corner. This module is still present from the original antenna installation, and had not yet received the high-pass filter retrofit as of this writing.

3 Tests and Methods

To better understand the loss of sensitivity and the three bandpass effects described in §1 and shown in Figure 3, and to assess the usefulness of placing slope-equalizing filters in the signal path, we designed a series of on-the-sky observations supplemented by laboratory tests.

3.1 The slope-equalizing filters for the 1-2 GHz IF signal passband

Earlier numerical manipulation of laboratory data had indicated that slope equalization may mitigate two of the three problems, namely slope and shoulder. In practice, this would be achieved by placing slope-equalizing filters in the signal path between the downconverter and the sampler.

Two models of slope-equalizing filters were purchased: one with a nominal slope of 3 dB/GHz, and one with a nominal slope of 8 dB/GHz. Measured residual slopes were 4 dB/GHz and 7.5 dB/GHz, respectively. Figure 9 shows laboratory measurements of the two equalizing filters, plotted with the unequalized response of the T304 1-2 GHz output.

Laboratory tests showed that the 3 dB/GHz equalizer was effective at removing the slope and mitigating the shoulder in window 3, while the 8 dB/GHz equalizer had the same effect upon window 4. On-the-sky test observations with the EVLA, as discussed in the following sections, confirmed the laboratory results but uncovered additional unanticipated and undesirable effects.

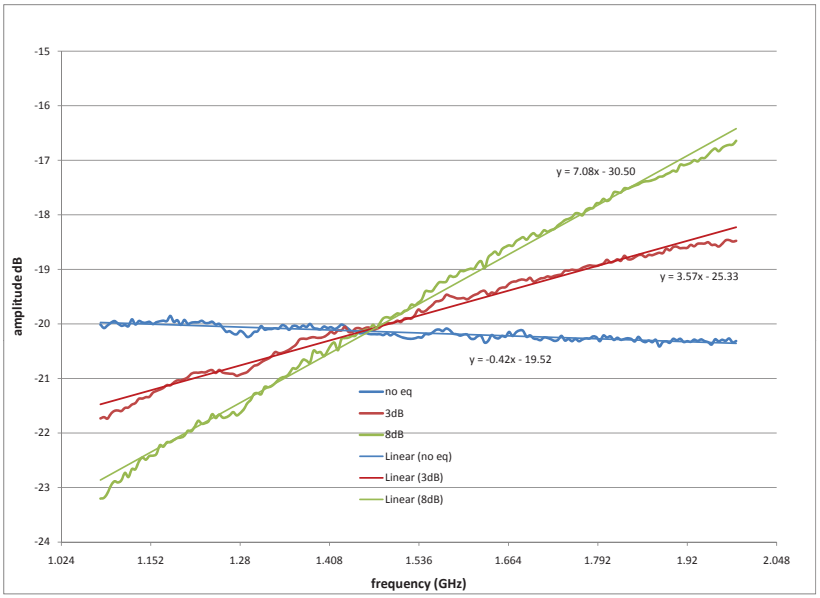

Figure 9: The frequency response of the two slope-equalizing filters. The blue trace shows the inherent slope in the passband. The red trace shows the 3 dB/GHz filter, and the green trace shows the 8 dB/GHz filter. The curves designated as *linear* in the figure legend are best fit lines to the data.

3.2 On-The-Sky Observations and Data Reduction

On March 15, 2011, we performed two sessions of on-the-sky test observations using 8 EVLA antennas equipped with Ku-band receivers. Each session lasted a total of 50 minutes. Both were identical except for the addition of slope-equalizing filters in the 2nd session. The four 1 GHz windows of the T304 were accessed sequentially according to the frequency settings listed in Table 2. A 1 MHz shift in the sky frequency was introduced between each consecutive frequency setting for ease of distinction.

Window	Intermediate Frequency (MHz)	1st LO Frequency (MHz)	2nd LO Frequency (MHz)	Sky Frequency (MHz)
1	7950-8974	12416	11022	15858-16882
2	8975-9999	12928	12047	15857-16881
3	10000-11024	13440	13072	15856-16880
4	11025-12049	13952	14097	15855-16879

Table 2: The four 1 GHz windows, the LO frequencies, and the corresponding sky frequencies of the Ku-band observations.

For each of the four settings, the WIDAR correlator was configured to deliver eight 128 MHz-wide subbands, each with 64 spectral channels and all four polarization products. The calibrator source J2202+4216 ($S_{16\mathrm{GHz}}$ ~4.65 Jy) and a blank field 1° away from the calibrator were observed in alternating scans for a total of 11 minutes per setting. The slope-equalizing filters were added to the 8 EVLA antennas for the second observing session. The 3 dB/GHz and 8 dB/GHz filters were installed on the RCP and the LCP, respectively, of the baseband pair AC (hereafter IFs A and C). Both types of filters have 9 dB of insertion loss that was compensated by increasing the power levels in the second observing session.

The data were loaded into AIPS, and the delays were corrected for each of the four 1 GHz windows in each observing session independently. Antenna-based bandpass calibration solutions

were obtained for each subband in each 1 GHz window using the calibrator J2202+4216 after properly accounting for its spectral index, which is $\alpha = -0.17$ (adopting $S \propto \nu^{-\alpha}$) between 8.4 and 18.2 GHz. The delay and bandpass calibration solutions were applied on the visibilities of the blank field, which were then used to measure the RMS noise values by fitting Gaussian functions to their histogram distributions.

Visibilities associated with certain antennas in certain windows showed non-Gaussian noise distributions, and were therefore excluded from the RMS noise measurements of both observing sessions, even if the trend was seen in only one of the observing sessions.

4 Results and Discussion

In the following sub-sections, we present on-the-sky and laboratory results for each of the three effects separately.

4.1 Asymmetry

On-the-sky observations show that the power between 1024 and 1054 MHz of the sampled signal (e.g., the 1st 30 MHz of subband 0 of the Ku-band observations) decreases faster with frequency than the power between 2018 and 2048 MHz (e.g., the last 30 MHz of subband 7 of the Ku-band observations). Figure 10 shows the normalized noise across subbands 0 and 7 of the 1st 1 GHz window (LO=11022) of IF A prior to the installation of the slope-equalizing filters. Subband 7 has a reversed channel order in this figure to enable comparison of sensitivities at the two extreme edges of the 1 GHz window. The data points are obtained by (1) measuring the RMS noise of each channel in subbands 0 and 7 using the data of the blank field, and (2) normalizing these measurements by the corresponding average of the RMS noise values measured using the central 10 channels (20 MHz) of each subband respectively.

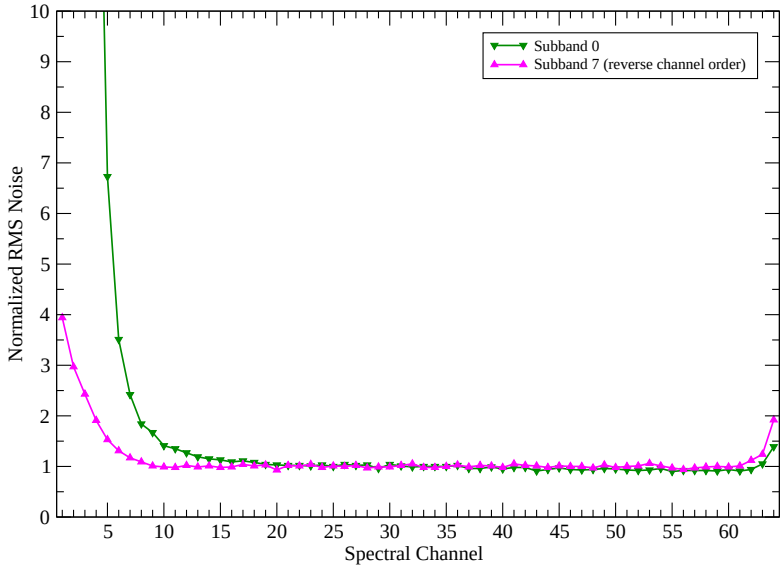

Figure 10: The normalized noise across subband 0 and 7 of the 1st 1 GHz window of IF A prior to the installation of the slope-equalizing filters. Subband 7 has a reversed channel order to show the loss of sensitivity at the two extreme edges of the window.

The loss of sensitivity in Figure 10 includes both asymmetry and shoulder components. The asymmetry component comprises contributions from both the anti-aliasing filter and the WIDAR

subband 0 FIR filter. These cannot be decomposed using the complete system (i.e., through observations). However, laboratory measurements were able to identify the part of the asymmetry component which is a feature of the anti-aliasing filter.

The 1-2 GHz anti-aliasing filter was specified to have a 1 dB bandwidth of 410 MHz (1331 to 1741 MHz) and a 15 dB bandwidth of 1024 MHz. These can vary by ±10 MHz from one edge of the filter to the other, and from one filter to another. This is common to all EVLA anti-aliasing filters. Figure 11 shows laboratory data for a typical anti-aliasing filter. The filter response has been folded over f=1536 MHz in order to enable comparison between the high and low frequency edges. Within a 30 MHz range, points measured from the 2 GHz edge (DC edge; red curve) are consistently worse by 60-70% compared to the corresponding points measured from the 1 GHz edge (blue curve). The amplitude in the 2 GHz edge is about 60% that of the 1 GHz edge throughout the filter transition.

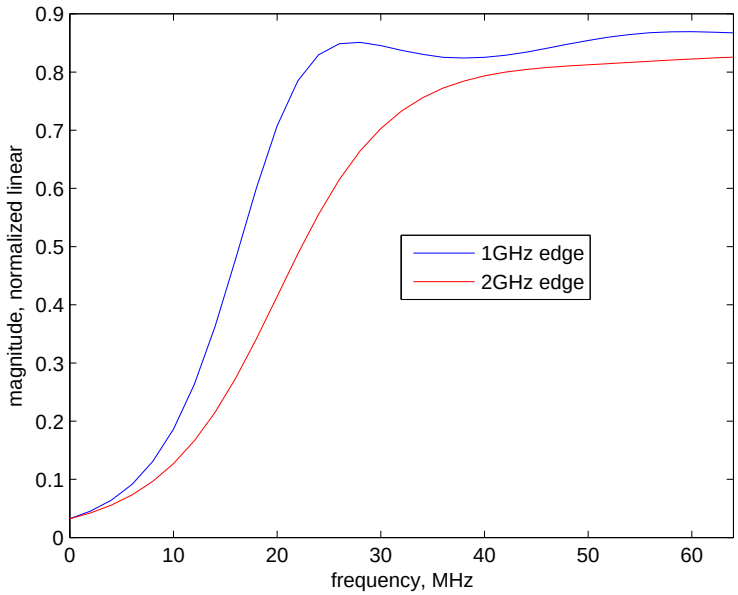

Figure 11: Anti-aliasing filter asymmetry. Red trace (2048 MHz, subband 0 edge) has been mirrored and overlaid on the blue trace (1024 MHz, subband 7 edge). Roll-off on the 2048 MHz edge is steeper than on the 1024 MHz edge.

The WIDAR subband 0 filter shows an increased roll off on its DC edge (Figure 12). It is presently an asymmetric bandpass filter which preferentially inhibits the DC component. The frequency response of the WIDAR subband 0 filter multiplies that of the anti-aliasing filter at the DC edge, producing the asymmetry seen in the rms noise shown in Figure 10.

The anticipated final WIDAR subband 0 filter consists of a lowpass filter at 128 MHz plus a mean-subtraction algorithm that will remove the DC component but leave the lower edge of the band intact. A plot of the frequency response of all 8 WIDAR subband filters is shown in Figure 13. The inset shows the frequency response of the present subband 0 filter in red, and the anticipated lowpass filter in blue.

4.2 Shoulder

As noted in §1, the shoulder effect is a pronounced roll-off on the 2 GHz edge of the band (subband 0; Figure 3). To assess whether slope equalization can correct for the shoulder, we now report the effect of adding the slope-equalizing filters (see §3.1) to the signal path.

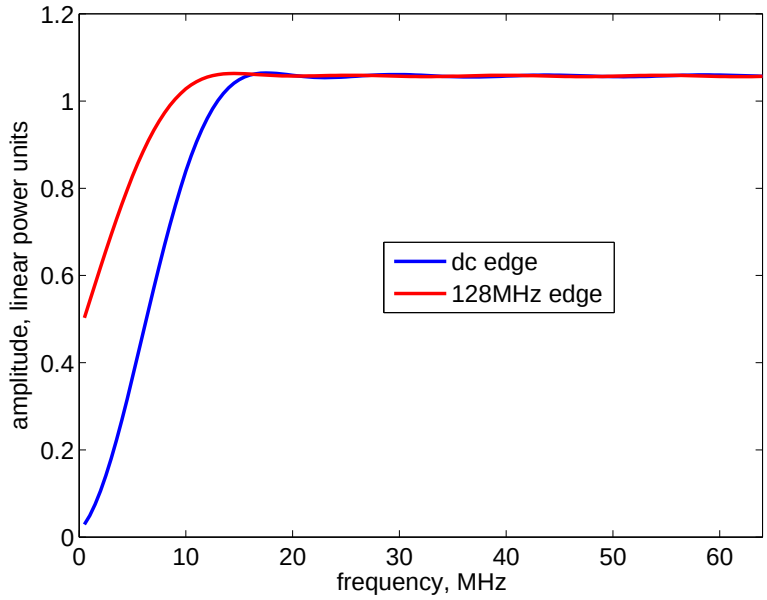

Figure 12: Frequency response of the WIDAR subband 0 filter. The 128 MHz edge of subband 0 (blue trace) has been mirrored and overlaid on the DC edge of subband 0 (red trace). Roll-off on the DC edge is steeper than on the 128 MHz edge.

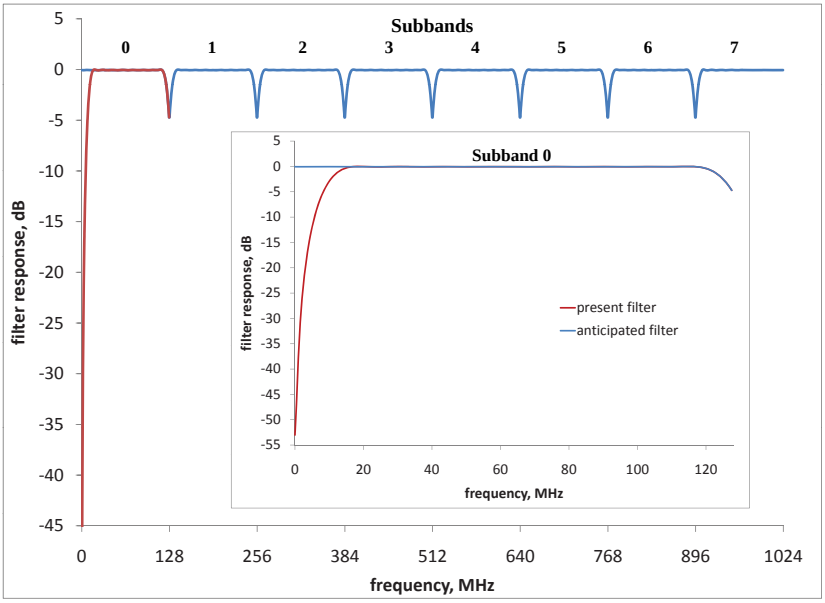

Figure 13: Frequency response of all 8 WIDAR subband filters, with the inset showing the frequency response of the current subband 0 filter in red and that of the anticipated subband 0 filter in blue. Note the asymmetric rolloff on the DC edge of the subband 0 filter.

Figure 14-*left* show the bandpass shapes of IFs A (*top*) and C (*bottom*) of antenna EA10, obtained using the data of the calibrator source J2202+4216 in the Ku-band observations, before the installation of the slope-equalizing filters. Each plot shows the four windows overlaid (Table 2), and their 1 GHz coverage divided into eight 128 MHz-wide subbands. For each of the four windows, the amplitude gains of all eight 128 MHz-wide subbands were normalized by the gain values obtained

using the central 10 channels (20 MHz) of their respective subband 7.

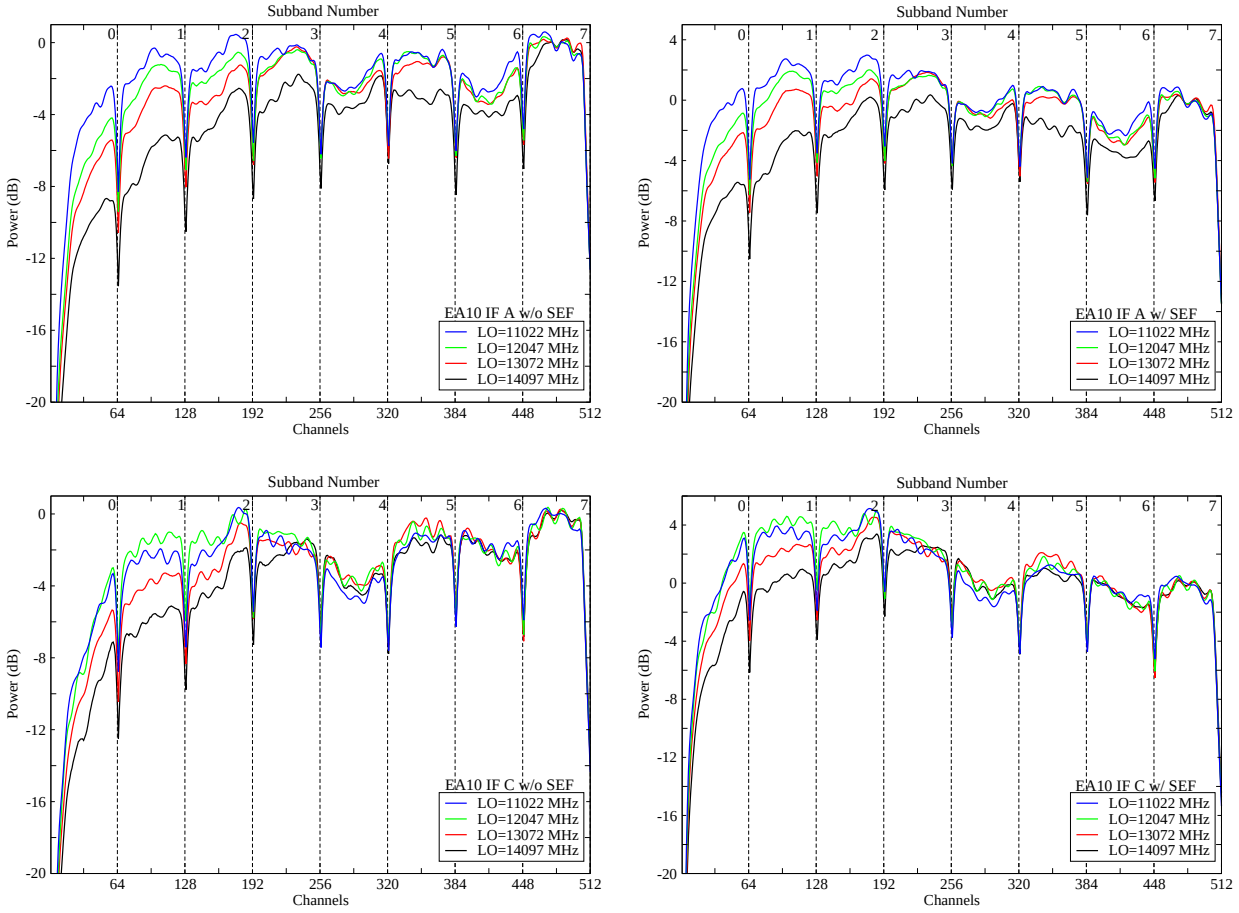

Figure 14: *Left:* The bandpass shape of the four 1 GHz windows of IFs A (*top*) and C (*bottom*) of antenna EA10 before the installation of the slope-equalizing filters (SEF). *Right:* The bandpass shape of the four windows of IFs A (*top*) and C (*bottom*) of antenna EA10 after the installation of the slope-equalizing filters (SEF). The amplitude values have been normalized using the central 10 channels (20 MHz) of subband 7 in each window.

Figure 14-*right* shows bandpass plots similar to those noted above, but obtained using the data after the installation of 3 dB/GHz and 8 dB/GHz filters on IFs A (*top*) and C (*bottom*), respectively. This resulted in an apparent improvement in the bandpass plots, including the shoulder effect in subband 0. To quantify this, we have compared the RMS noise level in subband 0 before and after the addition of the slope-equalizing filters.

The RMS noise has been measured for both Ku-band observing sessions (i.e., before and after installing the slope-equalizing filters) using the calibrated data of the blank field in each spectral channel of subband 0 in each window. The following have been performed:

1. Measuring the average of the RMS noise in the central 10 channels (20 MHz) of subband 1 of each window for IFs A and C, and for each observing session, separately.

2. Measuring the RMS noise of each channel in subband 0 of each window for IFs A and C, and each observing session, separately.

3. Normalizing the RMS measurements of the channels in subband 0 (obtained in step 2) by the

average of the RMS noise values of the central 10 channels (20 MHz) of subband 1 (obtained in step 1) for each window, IF, and observing session, separately.

4. Computing the ratio of the normalized RMS noise values by dividing the values obtained from the data without the slope-equalizing filters by the values obtained from the data with the slope-equalizing filters for each window and each IF, separately.

5. Applying a 3-channel smoothing to the ratio of the normalized RMS noise values derived in step 4 above.

Figure 15 shows these ratios with IF A (black) and IF C (red) for all four windows. These plots clearly demonstrate that the sensitivity is improving in the lower 50-70 MHz in each window by up to a few 10s of percent at the lowest edges. The largest improvement in sensitivity is seen in subband 0 of the 4th window (LO=14097 MHz), which reaches ∼32% toward the edge.

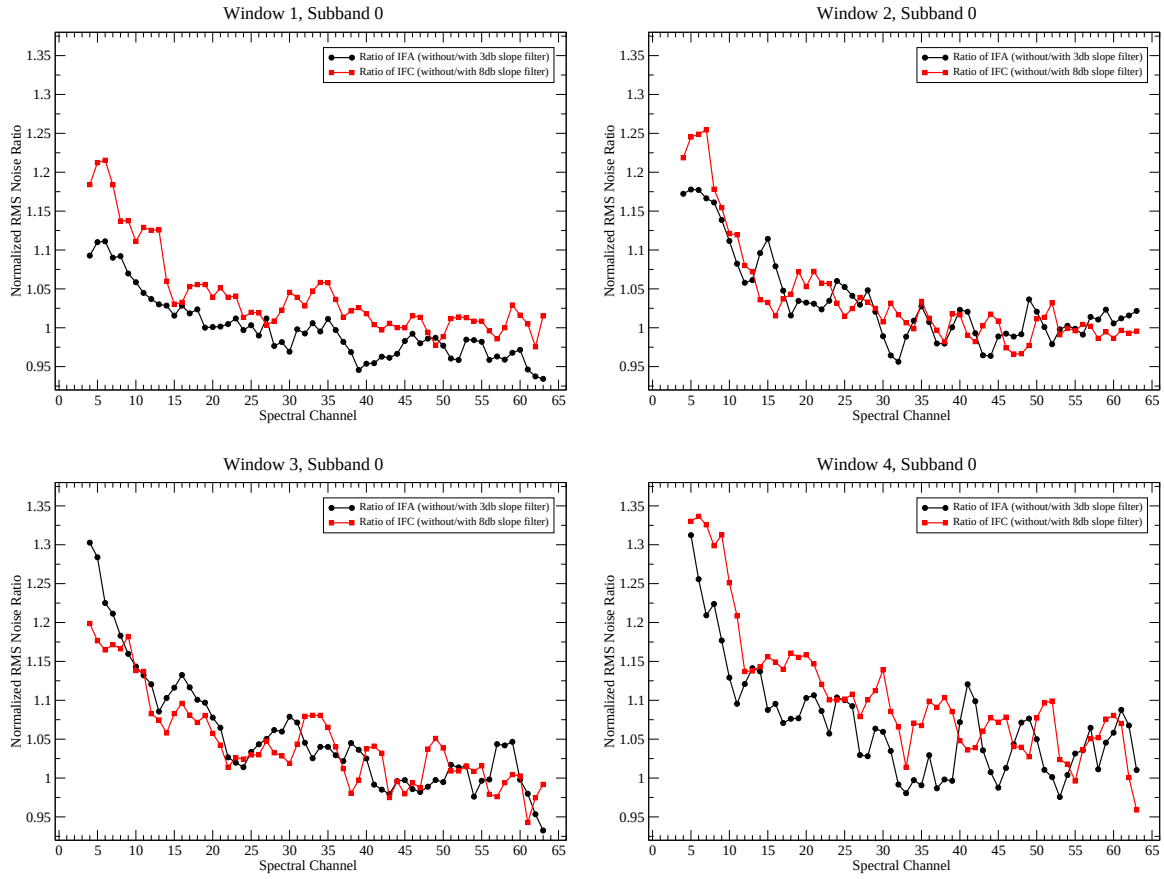

Figure 15: Three channel smoothed normalized RMS noise ratios of the Ku-band data before and after installing the slope-equalizing filters of subband 0 in each 1 GHz window. The normalization was done by the average RMS noise values of the central 10 channels (20 MHz) of subband 1 of the respective 1 GHz window, IF, and observing session.

4.2.1 The origin of the shoulder effect

The shoulder effect that appears towards the 2048 MHz edge (subband 0) of the output passband manifests as a steeper roll-off of about $6-8$ dB relative to the 1024 MHz edge. A portion (∼2 dB)

of this is attributable to the introduction of the narrower highpass filter (discussed in §2), which is exaggerated by the shoulder effect (see §4.3).

Further laboratory tests proved that the digitizer was not adding significantly to the shoulder effect. Figure 16 shows noise injected directly into the sampler (blue trace) and noise converted through the T304 (red trace). The shoulder is absent from the blue trace.

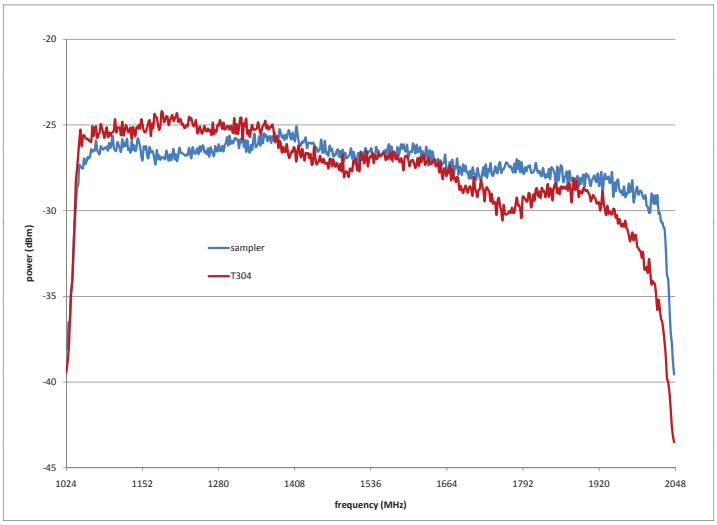

Figure 16: Expected bandpass shape: The blue trace shows noise injected directly to the digitizer through the anti-aliasing filter. The red trace shows the T304 output injected into the digitizer. The shoulder effect is present only in the T304 signal.

4.3 Slope

As noted in §1, the slope effect is a general downward slope across the passband that increases as we move from window 1 to window 4 (Figure 3). The addition of slope-equalizing filters, as seen in Figure 14-*right*, resulted in an apparent improvement in the slope across the entire 1 GHz band. To quantify this, we have compared the RMS noise level in each subband of each window before and after the addition of the slope-equalizing filters.

The RMS noise has been measured for both Ku-band observing sessions (i.e., before and after installing the slope-equalizing filters) using the calibrated data of the blank field in the central 10 channels (20 MHz) of each of the eight 128 MHz-wide subbands. The ratios of before to after are presented in Figure 17 for both IFs A (black) and C (red).

The 3 dB/GHz filters installed on IF A (black) resulted in a loss of sensitivity between 6 and 11% across the four 1 GHz windows. In any window, the sensitivity loss across subbands is mostly flat and within 4%. Excluding subband 0 of window 4, the 8 dB/GHz filters installed on IF C (red) resulted in a loss of sensitivity between 0.5 and 9.5% across all windows and subbands.

The reasons for the loss of sensitivity after adding the slope-equalizing filters remain unknown. However, it is clear that adding these filters has degraded the sensitivity throughout the four 1 GHz windows, with the exception of a single subband (subband 0) in a single window (window 4) and only for a single filter (8 dB/GHz).

4.3.1 The origin of the slope effect

The T304 frequency response is not entirely flat over the entire input band. The response from 8-10 GHz is reasonably flat. Above 10 GHz, a slight slope is introduced that degrades even further

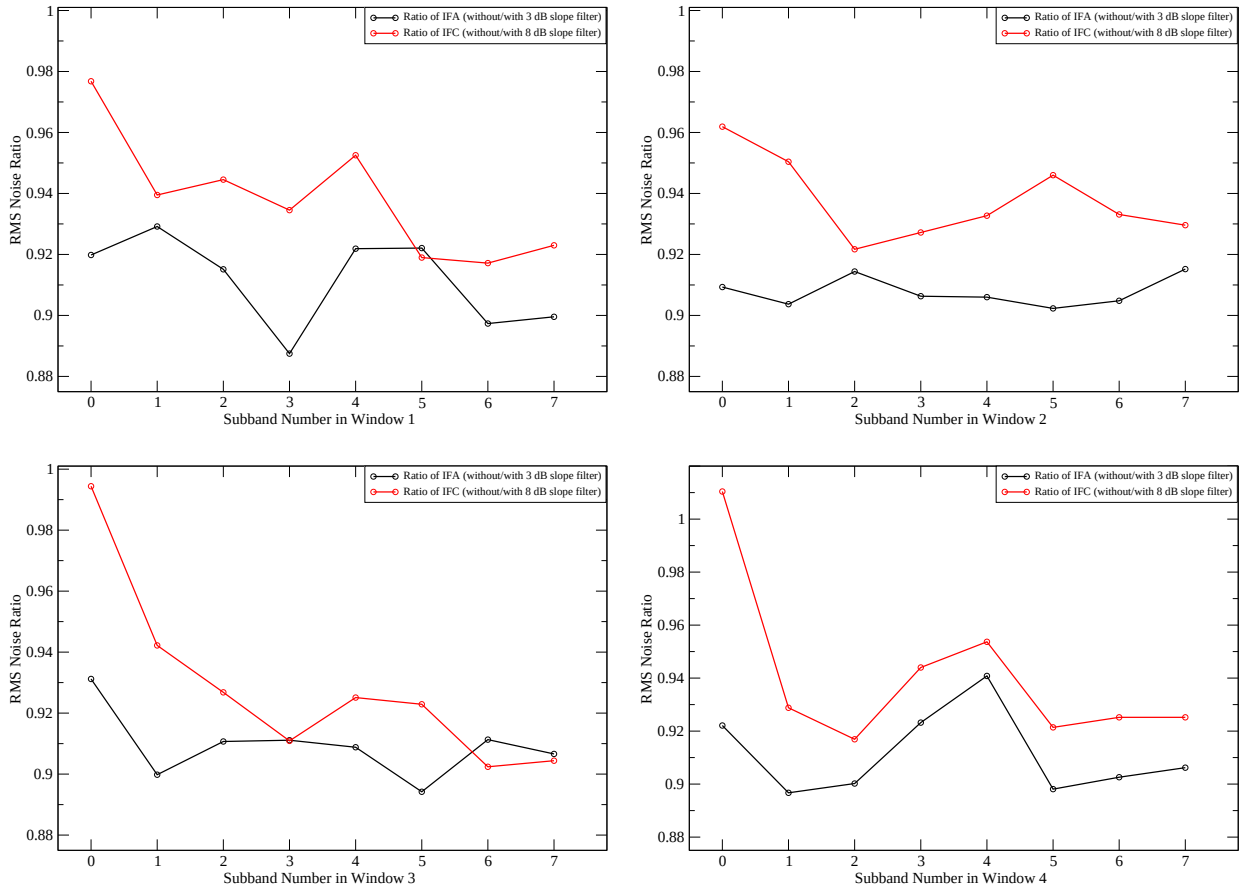

Figure 17: The RMS noise ratios of the data before and after installing the slope-equalizing filters of all eight subbands in each 1 GHz window. The points are obtained by using the central 10 channels (20 MHz) from each subband.

from 11-12 GHz. Figure 18-*left* shows this effect referred to the input frequency, while Figure 18-*right* shows the relative slopes and levels of the four windows as measured at the output of the T304. The effect appears to be the cumulative contributions of electronic components, circuit board material, cabling, and impedance mismatch throughout the IF system.

T304 modules in the field are assembled using Printed Circuit Boards (PCBs) from two different vendors. Tests show that the slope effect is exaggerated in the circuit boards from one vendor (Circuit Design Specialties; CDS) compared to the other (Trilogy Circuits). This in turn appears to further magnify the shoulder effect in the CDS boards. The manufacturer of the laminate material for both sets of PCBs, Rogers Corporation, has been contacted in an effort to understand the cause of this discrepancy. Figure 19 shows the relative gain, slope, and shoulder variation for representative samples of the two sets of PCBs.

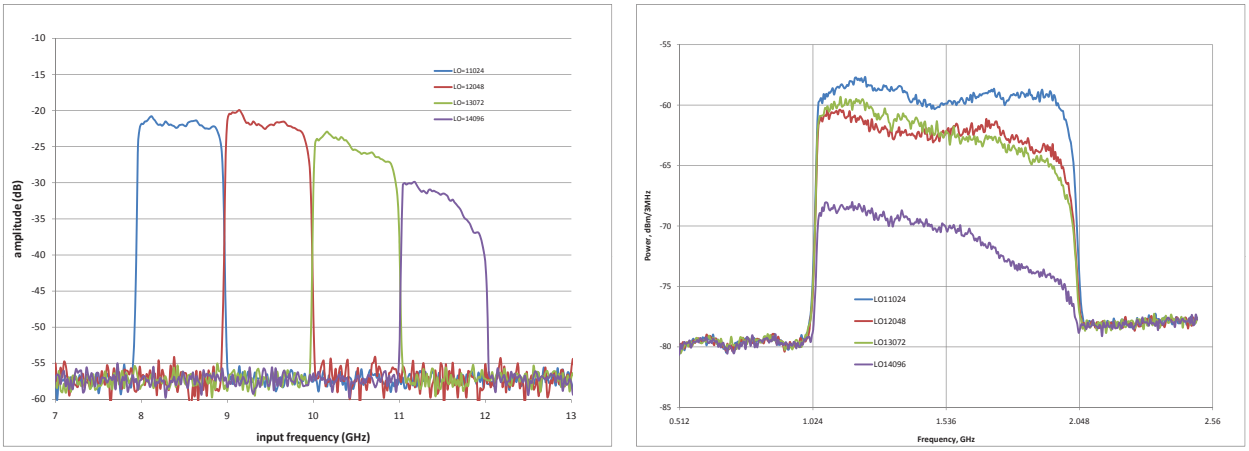

Figure 18: *Left*: Each of the four 1 GHz windows that comprise the T304 input passband. *Right:* Each of the four windows overlaid to show relative slope and shoulder effects.

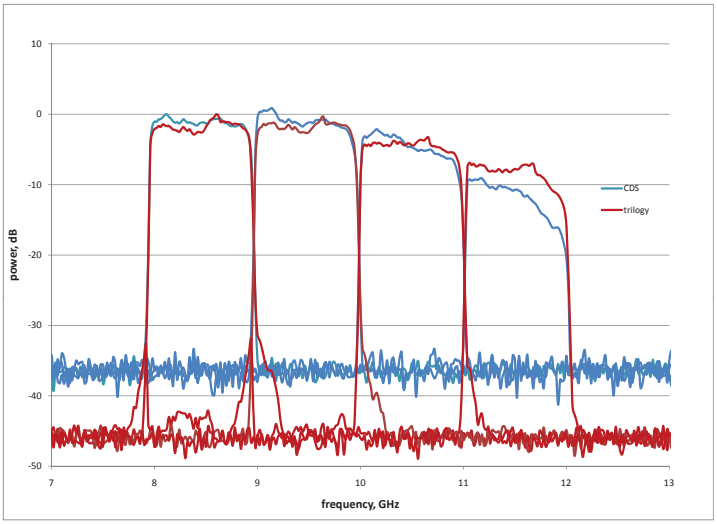

Figure 19: The four 1 GHz windows as measured through PCBs from two different manufacturers. Approximately two-thirds of the T304s are built with PCBs from Circuit Design Specialties (CDS; blue trace), while the remainder are built with boards from Trilogy Circuits (red trace). A dozen or so modules are hybrids of the two. The slope and shoulder effects are exaggerated in the CDS boards.

5 Conclusions

We have attempted to decompose the larger problem of the sensitivity degradation in the 1-2 GHz IF passband into:

1. a general slope across the band that increases with increasing T304 input frequency,
2. a premature roll-off (shoulder) at the 2 GHz end of the passband that is introduced by the 1900 MHz highpass filter and is exaggerated by the slope effect, and
3. an asymmetry in the cascaded responses of the anti-aliasing filter and WIDAR subband 0 FIR filter that affect the outer 30 MHz of the band.

The RMS noise degradation occurs most significantly in subband 0 of the 4th 1 GHz window. Given current default LO tunings, this will primarily affect EVLA L-band observations, but will also affect observations that use the top 1 GHz of the X-band receiver with the 8-bit signal path. However, at X-band, wideband continuum observations are best performed with the 3-bit signal path, which avoids the section of the T304 that introduces the shoulder effect. For L-band, three strategies could help to improve the performance and/or avoid the problem in this region:

1. Use more of the 8 bits for the representation of the sampled data. This will decrease dynamic headroom in the sampler, thereby increasing vulnerability to RFI, but may enable better overall signal-to-noise ratio for RFI-free channels.

2. Considering that the EVLA antennas have two 8-bit samplers per polarization, tune the LOs such that the full bandwidth of L-band is covered by these two samplers while avoiding the shoulder (i.e., avoiding subband 0).

3. Implement the anticipated, final version of the subband 0 FIR filter plus DC-removal algorithm. This will remove about half of the asymmetry in the band edge.

We have also studied the effects of a potential mitigating action: the addition of the slope-equalizing filters. While the sensitivity increased in certain channels of subband 0, the overall sensitivity of the band was degraded. Both the slope and the shoulder effects were apparently reduced in bandpass plots, but the RMS noise increased in almost all cases.

To the extent that T304 circuit board material and manufacturing process is contributing to the slope effect, we are seeking the help of the material manufacturer to study the cause of the behavior. To the extent that the highpass filter in the T304 has contributed to the shoulder effect, we are investigating the possibility of a custom-designed filter that may meet both the image-rejection and bandpass variation specifications simultaneously. Any solution that involves replacing components within the T304 is guaranteed to be both expensive and time-consuming.

6 Acknowledgements

We would like to thank K. Sowinski, R. Long, D. Scott, J. Langevin, E. Chavez, and the EVLA operators, for assisting with the acquisition of the data, and R. Perley and J. Jackson for their valuable inputs to the analysis and discussion of the results presented in this memo.